NRC Research Press

ARTICLE

Assessment of wind speeds based on damage observations from the Angus (Ontario) Tornado of 17 June 2014

Gregory A. Kopp, Emilio Hong, Eri Gavanski, Derek Stedman, and David M.L. Sills

Abstract: A tornado occurred in Angus, Ontario, during the late afternoon hours of 17 June 2014. The authors conducted a damage investigation on the morning following the storm. The damage indicators support the classification of the tornado as an EF-2 on the Enhanced Fujita Scale, including the observation of several complete roof failures of recently-constructed, wood-frame houses. Most of the damage to residential homes was contained along two streets, with the tornado appearing to have gone down the backyards between the two. In total, 101 houses were observed to have sustained some level of damage. The evidence suggests that the quality of construction likely affected the performance of failed roofs. A detailed fragility analysis was conducted to assess wind speeds associated with these failures of the roof-to-wall connections. An overturned and lofted box truck provided the opportunity to correlate this failure with adjacent, repetitive failures of roof sheathing, shingles, and garage doors.

Key words: tornadoes, EF-Scale, wood-frame houses, low-rise buildings, wind loads.

Résumé : Une tornade s'est produite à Angus en Ontario, au cours des dernières heures de l'après-midi du 17 juin 2014. Les auteurs ont mené une enquête sur les dommages le lendemain matin de la tempête. Les indicateurs de dommage confortent la classification de la tornade comme « EF-2 » sur l'échelle de Fujita améliorée, y compris l'observation de plusieurs défaillances totales de toit de maisons à charpente de bois construites récemment. La plupart des dommages aux résidences étaient confinés le long de deux rues, du mê me coup la tornade semblait avoir descendu les arrière-cours entre les deux rues. Au total, on a observé 101 maisons ayant subi un certain niveau de dommage. Les données montrent que la qualité de la construction a vraisemblablement eu une incidence sur le rendement des toits endommagés. Une analyse en détail sur la fragilité a été réalisée afin d'évaluer les vitesses du vent associées aux défaillances des raccordements toit-murs. Un camion à caisson renversé et projeté en hauteur a fourni l'occasion de corréler cette défaillance aux défaillances adjacentes et répétitives de voligeages, de bardeaux de toit et de portes de garage. [Traduit par la Rédaction]

Mots-clés : tornades, échelle de Fujita améliorée, maisons à charpente en bois, bâtiment bas, surcharges dues au vent.

Introduction

Wind speeds in tornadoes are rarely measured; rather, they are assessed indirectly by examining the damage following the storm and estimating the wind speeds that could have caused the damage. The original basis for this was the Fujita Scale (Fujita 1971), which was modified into the Enhanced-Fujita Scale (EF-Scale) by Texas Tech University (WSEC 2006). One of the strengths of Fujita's original scale was how it grouped typical damage observations. For example, for F2 tornadoes, the scale indicates that there should be "considerable damage [including] roofs torn off frame houses; mobile homes demolished; large trees snapped or uprooted … cars lift off ground." In the Fujita Scale, this level of damage falls into a wind speed range of 190–260 km/h (3 s gust speeds; see WSEC 2006 for details). However, it was generally accepted that there were some issues with this scale, particularly with the wind speeds at the high end of the scale, a lack of recognition of differences in construction, and over-simplification of the damage descriptions (SPC 2016). The Enhanced-Fujita (EF) Scale attempted to address these. The EF-Scale reduced the wind speeds at the top of the scale significantly, brought in many more Damage Indicators (DIs), and introduced the concept of Degrees of Damage (DODs), which are the possible states of damage for each DI (WSEC 2006).

Table 1 provides the DOD descriptions for one- and two-family residences (100–500 m^2), which correspond to typical North American, wood-frame houses. Table 2 provides the EF-Scale wind speeds, as adopted in Canada. Note that Canada uses a modified version of the United States (US) EF-Scale (WSEC 2006), with slightly different wind speeds and additional and revised DIs and DODs (Sills et al. 2014).

Included with DOD tables for each of the DIs are estimated wind speed ranges, which were obtained by an 'expert elicitation' process (WSEC 2006; Mehta 2013). For example, for the one- and two-family residences shown in Table 1, DOD-6 is "Large sections of roof structure removed; most walls remain standing" with an expected wind speed of 195 km/h, a lower-bound wind speed of 165 km/h, and an upper-bound of 230 km/h. For this particular DOD, the WSEC (2006) report states that "if only the roof structure of the two-story residence is uplifted by a storm and the exterior walls remain in place (DOD-6), the expected wind speed of the storm at that location is estimated to be 122 mph [198 km/h]. The reported value could vary from 104 to 142 mph [169 to 230 km/h] depending on circumstances. Large overhangs (greater than [0.6 m]), improper toe nailing (two nails instead of three) … would suggest a wind speed less than 122 mph [198 km/h] but not less than 104 mph [169 km/h]. Use of hurricane clips … suggest a wind speed

Received 12 May 2016. Accepted 19 October 2016.

G.A. Kopp, E. Hong, and D. Stedman. Boundary Layer Wind Tunnel Laboratory, Faculty of Engineering, University of Western Ontario, London, ON N6A 5B9, Canada.
E. Gavanski. Department of Urban Engineering, Osaka City University, Osaka, Osaka, 558-8585, Japan.
D.M.L. Sills. Cloud Physics and Severe Weather Research Section, Environment and Climate Change Canada, Toronto, ON M5H 5T4, Canada.
Corresponding author: Gregory A. Kopp (email: gakopp@uwo.ca).

Table 1. Degree-of-damage (DOD) descriptions and expected wind speeds for one- and two-family residences (100–500 m^2), as adopted in Canada.

Degree-of-damage	Damage description	Expected value (km/h)	Lower bound (km/h)	Upper bound (km/h)
1	Threshold of visible damage	105	85	130
2	Loss of roof covering material (less than 20%), gutters and (or) awning; loss of vinyl or metal siding	125	100	155
3	Broken glass in doors and windows	155	125	185
4	Uplift of roof deck and loss of significant roof covering material (20% or more); collapse of chimney; garage doors collapse inward; failure of porch or carport	155	130	185
5	Entire house shifts off foundation	195	165	225
6	Large sections of roof structure removed; most walls remain standing	195	165	230
7	Exterior walls collapsed	210	180	245
8	Most walls collapsed, except small interior rooms	245	205	285
9	All walls collapsed	275	230	320
10	Destruction of engineered and (or) well-constructed residence; slab swept clean	320	265	355

Table 2. Comparison of the Fujita and EF-Scale wind speeds.*

Category	Fujita Scale (WSEC 2006)**, km/h	EF-Scale (Sills et al. 2014), km/h
0	70–125	90–130
1	125–190	135–175
2	190–260	180–220
3	260–335	225–265
4	335–420	270–310
5	420–510	315 or more

*Three second gust speeds.
**Rounded to nearest 5 km/h.

higher than 122 mph [198 km/h] but not greater than 142 mph [230 km/h]. The EF-Scale rating would be the category containing the estimated wind speed for this degree of damage." This will be examined in some detail in the current study.

Analysis of wind loads on houses in straight-line winds has been conducted since Jensen's (1958) pioneering research (see Surry 1999 for a discussion of Jensen's work). It is well known that, beyond the effects of roof-to-wall connections discussed by WSEC (2006; quoted above), terrain, roof and building shape, openings in the building envelope all affect the wind loads, and therefore, failure-inducing wind speeds, significantly. However, these parameters are not included in EF-Scale evaluations at present. It should be noted, however, that in Canada roof shape is partially considered since a note that goes with Table 1 states that for "hip roofs[s], increase toward upper-bound wind speed for DOD-4 and DOD-6."

Recent research has focussed on using highly detailed damage surveys to examine correlations of adjacent damage and assess possible wind speeds using recent research findings (e.g., Roueche and Prevatt 2013). The tornado in Angus, Ontario, on 17 June 2014 provides another opportunity for this. The Angus tornado occurred in an area with many residential, wood-frame houses. Many of the houses that were damaged had been recently constructed, typically less than three years old. As described below, the damage varied from shingle and siding failures to complete roof and wall failures, with a box truck that was lofted and overturned. The objective of this paper is to present the statistics of the damage observations, together with an emphasis on the correlation between repetitive failures with analyses of wind speeds based on boundary layer wind tunnel, full-scale component, and full-scale structural tests.

Damage observations

Overview of the storm

During the late afternoon hours of 17 June, intense thunderstorms developed in advance of a cold front moving through southern Ontario, spawning two tornadoes and a downburst. The most severe of these events was the tornado that began just west of Angus and continued to cause up to EF2 damage as it tracked east. The tornado dissipated shortly after it passed through the southwestern edge of the City of Barrie, having travelled a total distance of 20.8 km with a maximum width of damage of about 300 m. Three minor injuries were recorded. Insured losses were reported by the Insurance Bureau of Canada (2014) to be at least $30 million, mostly associated with damage in the Angus area.

Overview of the damage in Angus

Figure 1 shows the survey area within Angus and the locations of houses with damage. Much of the damage was located on two streets, Stonemount Cres. and Banting Cres., and that away from these two streets there was only scattered, light damage. The aerial photograph in Fig. 1*a* shows this clearly. In total, 101 houses were identified with visible damage. Figure 1 also shows that there were 11 houses that lost their roofs, and that these were located in close proximity to each other on Stonemount Cres. In addition, many (eight) of the roof sheathing failures occurred close to these complete roof failures on Stonemount Cres., with only three sheathing failures observed on Banting Cres. The difference in the damage level on these two streets is dramatic, as can be seen in Fig. 1*a*. It was observed that most of the debris was confined to the backyards between these two streets. The centre of the tornado track appeared to be between these two streets, but likely closer to Stonemount Cres.

The width of the most significant damage was estimated to be about 25–30 m, while the overall width of the threshold of damage in this area was about 200 m. Surrounding the surveyed area, tree damage was found both to the west and to the east of the highly damaged area, and tended to be in line with the damage through the backyards. The part of the tornado path that exhibited DOD-6 damage to houses in Angus (i.e., which is nominally EF-2) extended for about 300 m. Examining the damage patterns and movement of debris, it appeared as though the tornado core was quite narrow since the damage was mostly contained within the backyards. In fact, the debris from Banting Cres. houses did not appear anywhere on this street; rather, the sheathing and shingles went in a northerly direction (towards Stonemount Cres.), and almost certainly in a north-easterly direction. This is likely the source of debris that broke the windows on the south-side (backyards) of the Stonemount Cres. houses, discussed below. However, the fences and other debris originating in the backyards could also be the source of debris for these broken windows. We also note that there was some debris (not much, but some) on the north-side of properties on Stonemount Cres. This is consistent with a vortex translation speed that must have been relatively high compared to its rotational speed because of the convergent debris pattern, as suggested by Bunting and Smith's (1993) model for fast-moving tornadoes (see their fig. 4). Using the translation speed of the parent mesocyclone as a proxy leads to an estimated tornado translation speed of about 65 km/h (18 m/s). This,

Fig. 1. (*a*) Aerial photograph of the primary damage (source: Ian McInroy/Barrie Examiner, used with permission), and (*b*) a summary of all damage observations in Angus, ON, from survey of 18 June 2014 using an image from Google Earth. Red symbols indicate global roof failure, green symbols indicate roof sheathing failures (while the roof structure remained in place), and yellow symbols indicate all other damage. Note that construction was still occurring in this neighbourhood, so not all houses appear in the damage map. [Colour online.]

together with a damage width of about 200 m suggests a duration of high winds (i.e., above the threshold of damage) of about 10 s, at most, for any particular location.

As described above, there were a variety of different levels of damage found for the 101 houses identified with visible damage. Table 3 summarizes the observed damage. In the table, roof failure indicates the complete removal of the roof from the walls, i.e., failure of the toe-nailed, roof-to-wall connections (RTWC). When this type of failure occurs, the roof usually flies off of the walls. However, toe-nail failures do not always lead to flight of the roof, as shown in Kopp et al. (2012). Such failures can only be identified by examining connections within the house, which was not done in the current study. Debris impacts that cause large openings are often related to structural roof failures (Morrison et al. 2014) by elevating the internal pressure (Kopp et al. 2008). Here, 'debris impact' indicates the number of houses where there was impact damage (of any kind).

Structural roof failures

The most severe damage observed was roof structural failure. Houses that experience roof structural failure are usually condemned and demolished. Most of these also lose the majority of their contents due to rain and wind damage. Ten of the eleven houses with complete roof failure had the roof becoming detached and blowing off of the walls. On the other house, the roof was displaced, but did not blow off. The blown-off roofs travelled in an east-southeasterly direction, along with other debris, and, in some cases, impacted adjacent houses. In all of the houses that had complete roof failure, there was at least one broken window on a single wall (on their south-side in the backyard), which appears to have played a significant role in these failures, as discussed below.

As seen in Figs. 1 and 2, many of the houses that lost their roofs were adjacent to each other indicating that the wind speeds were consistently above the threshold for this failure at this location. In addition, the authors examined the connections for all of the failed roof trusses that could be identified on the ground (and from high-resolution photographs of those remaining on the roof that could be seen from the street or backyard) and it was found that practically all of the toe-nailed roof-to-wall connections (RTWC) were below code requirements, with cases of zero, one, and two nails in the connections, rather than the code-required three. However, only a relatively small number of RTWC could be definitively identified, so any conclusions based solely on this evidence is tentative. (There is additional evidence of poor construction quality associated with wall failures, which is discussed further below.) Figure 3 shows an example of one roof truss, with evidence of only a single nail being used in the connection. Thus, improperly toe-nailed RTWC undoubtedly played a role in (at least some of) the roof failures.

Further evidence for issues with quality of construction is provided in Fig. 4, which shows one of the structural wall failures. In this case, the second-floor wall was not fastened to the floor and it is likely that the pressure caused by wind sucked the unfastened wall outwards. A similar issue was found for the wall failure in Fig. 2, although the number of fasteners could not be identified.

Table 3. Summary of damage observations.

Damage observation	DOD	Quantity
Roof structural failure	6	11
Roof sheathing	4	11
Garage doors	4	9
Porch columns	4	4
Broken windows	3	23
Shingles	2	32
	4	16
Fascia/soffits/eaves	2	36
Siding	2	28
Walls (structural)	—	9
Bricks	n/a	4
Debris impact	n/a	38
Box truck lofted/overturned	n/a	1
Total houses		101

Fig. 2. House with observed roof and wall failure (source: the authors). [Colour online.]

Fig. 3. Roof truss from a house with a structural roof failure. This roof truss had only one toe-nail in the connection, rather than the code-required three (source: the authors). [Colour online.]

Fig. 4. Wall failure due to missing inter-storey connections (source: the authors). [Colour online.]

In total, there were 38 houses that were observed to have experienced debris impact damage. This category varied with some houses taking heavy damage from many pieces of debris, while others had less damage. In total, there were eight houses that clearly experienced debris impact from large portions of roofs. Impacts to siding and windows were common among the houses along the storm track. In total, 23 houses had window damage (and higher numbers had siding damage). Of particular note is that all houses that had complete roof failure had broken window(s) on one wall. Siding damage consisted of numerous cuts, tears, and dents, with roof structural members often penetrating the walls.

Roof sheathing, shingles, and garage doors

Of the remaining damaged houses (i.e., not counting those with structural roof failure), 11 had at least one roof sheathing panel failure. Variable numbers of panels failed, with about a third of the houses losing only one panel and another third losing multiple panels. Houses with similar numbers of panel failures were grouped closely together with many of the houses having missing panels being located near houses that had lost their roof. This indicates that the tornado wind speeds may have been more intense in these locations or that the construction quality issues also applied to the sheathing. However, examining the sheathing panels found in the debris, the nail sizes exceeded the code minimum values of 51 mm (6d) in length, with mostly 63 mm (8d) nails found. The failed-panel locations on the roof varied from house to house; however, there were some similarities between adjacent houses, with some repeated patterns. These patterns were more pronounced with the shingle loss than the sheathing loss (due to greater numbers). Figure 1*a* shows that there was a repetitive pattern of shingle failures on Banting Cres., which suggests that the wind speed was fairly constant along the bulk of this street. On the front side of these houses, nine garage doors were observed to have failed. Examining the debris field, it appears probable that these failures were due to pressure and not to debris impacts.

Regarding the repetitive failures of shingles, sheathing and garage doors, DOD-4 indicates "uplift of roof deck and loss of significant roof covering material (20% or more); collapse of chimney; garage doors collapse inward; failure of porch or carport." This is precisely what has been observed on Banting Cres. The EF-Scale suggests that this level of damage is associated with wind speeds in the range from 130 to 185 km/h, and an 'expected' value of 155 km/h (Table 1). This is in the EF-1 range of wind speeds (Table 2), an issue that is examined further below.

Vehicles

One of the interesting failures in Angus was a U-Haul box truck that was overturned by the wind. In fact, the evidence suggests that the truck was lofted, clipping one car as it went over two parked cars in the adjacent driveway, as illustrated in Fig. 5. The truck's ramp remained on the front lawn suggesting that the vehicle had been parked there. Like for the flight of the roofs, the direction of the truck motion was in an east-southeasterly direction. No evidence of sliding was observed. Limited experimental evidence suggests that lofting a vehicle requires higher wind speeds than sliding or overturning (Haan et al. 2011). No other vehicles were observed to have moved in the storm, although homeowners were not contacted about this.

Fragility analysis of roof failures

Overview of the approach

In this section, failure-inducing wind speeds for both roof sheathing and complete roof failures in Angus are estimated using a fragility-analysis approach.

Limit states

In the current analysis, failure for toe-nailed RTWCs is defined as failure of simultaneous, multiple RTWCs that have an effective area, A_E, over which they effectively act as a single unit. This assumption is consistent with damage observations discussed above and with full-scale laboratory experiments (e.g., Morrison et al. 2012; Henderson et al. 2013) and other analyses (e.g., Rosowsky and Cheng 1999). In the present analysis, the minimum effective wind area is assumed to be one-third of the length of the house, L_1, times half of the roof width, L_2, as shown in Fig. 6. The definition of wind direction, θ, employed in the wind tunnel test for the measurement of the pressure coefficients used for the calculation of wind loads are also presented in Fig. 6. Considering the wind directions suggested by the failure and debris flight observations, along with Bunting and Smith's (1993) model for fast-moving tor-

Fig. 5. Lofted and overturned U-Haul box truck with its likely direction of motion through the air indicated by the yellow arrows. The red circles indicate the ramp and for-sale sign while the orange circle indicates the location of greatest impact. Repetitive shingle, roof sheathing and garage door failures can also be seen in the photograph (source: Ian McInroy/Barrie Examiner, used with permission). [Colour online.]

Fig. 6. Tributary area definitions used for fragility analysis of roof-to-wall connection failures.

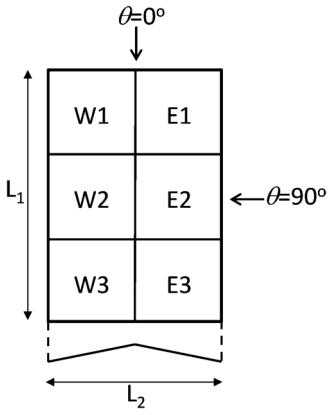

nadoes, roof failures were encompassed by the wind directions in the range provided in Fig. 6 (0 degrees, or easterly-winds for this tornado, through to 90 degrees, or northerly). Based on the RTWC failures observed in Angus, three combinations of the effective tributary area, L1 + R1, L1 + L2 + L3, R1 + R2 + R3 are considered.

The limit state function, z, can be written as

$$z = R - W + D \quad (1)$$

where R is resistance of the multiple RTWCs within the combined effective tributary area, W is wind load acting on the same area, and D is dead load. Failure occurs when $z < 0$.

Failure is defined similarly for the sheathing panels, using the same equation. However, the wind loads, resistance and dead loads are all modified to consider appropriate values for 1.2 m × 2.4 m plywood panels. In addition, a single sheathing panel failure is considered instead of multiple panel failures. This is because the change of internal pressure due to a sequential loss of sheathing panels cannot be correctly considered without many potentially unrealistic assumptions with the current analytical method, which does not consider the time series of tornado wind pressures.

Resistance statistics

Published experiments have revealed failure modes and capacities for toe-nailed RTWCs (e.g., Cheng 2004; Shanmugam et al. 2009; Morrison and Kopp 2011; Khan et al. 2012). Of particular interest for the current study, Morrison and Kopp (2011) applied ramp and realistic fluctuating wind loads to toe-nailed connections with sufficient numbers of specimens (approximately 20 for each loading rate) to examine failure mechanisms as well as to obtain statistically reliable capacities for both code-compliant connections (three nails per connection) and those with missing nails. These authors found that the toe-nail connection capacities are independent of loading rate, so the statistics for all of their ramp loading rates were combined for the current analysis. The resistance statistics for code-compliant connections are R_{0mean} = 2826 N, with a coefficient of variation (CV), R_{0CV} = 0.21, while values for RTWCs with missing nails are discussed below. (Note that, at the maximum tested loading rate of 32 kN/min used by Morrison and Kopp (2011), the mean capacity is reached in about 5 s, which is the same order of magnitude as the rate of load increase for this tornado.) In the current analysis, R_0 is modeled as a lognormal variate based on Akaike Information Criterion (AIC) and Bayesian Information Criterion (BIC) (Schwarz 1978). This results in the distribution function, $F(R_0)$, given by

$$F(R_0) = \Phi\left[\ln R_0 - \ln\left(1/\sqrt{1 + R_{0CV}^2}\right)\Big/\sqrt{\ln\left(1 + R_{0CV}^2\right)}\right] \quad (2)$$

where $\Phi(\bullet)$ denotes the standard normal distribution function (Melchers 1999). Since the sample value of resistance, R_0, using the statistics mentioned above is for individual RTWCs, the sample R in eq. (1) is obtained from $R = \Sigma R_{0,i}$, where the summation is over all RTWCs within the effective area, assuming that the truss spacing of the roof system is 0.6 m. This has the effect of reducing the variance of the roof capacity compared to that of individual connections (Rosowsky and Cheng 1999). With this assumed truss spacing, there will be six fasteners in the minimum effective wind area for gable roofs (e.g., L1 or R1) and non-corner hip roof zones (e.g., L2 or R2). In the corner zone for hip roofs (e.g., L1 or R1), there are 14 fasteners each.

The capacity of sheathing panels was based on the experimental results obtained by Henderson et al. (2013) and Gavanski et al. (2014), who examined sheathing panel failures by applying ramp and realistic fluctuating wind loads to 11.1 mm thickness OSB panels fastened to 2 × 4 timber trusses in several fastener arrangements and fastener types. Considering the fasteners found during the damage survey and the National Building Code of Canada (NBCC 2010), the analysis focussed on 6d and 8d spiral nails with spacing of 150 mm on-centre (o.c.) along edge supports and 300 mm o.c. along intermediate supports (which will be denoted as the '150/300' spacing in the rest of this manuscript). The sheathing panel capacity, R, is also modeled as a lognormal variate using eq. (2) with the statistical information of R_{mean} = 2670 Pa and R_{CV} = 0.14 for 6d spiral nails and R_{mean} = 4120 Pa and R_{CV} = 0.10 for 8d spiral nails.

Wind loads

To consider the net wind loading, external pressures acting on the exterior roof surfaces and internal pressure caused by a dominant opening on a wall are considered. In the present work, experimentally-measured wind loads, obtained in a boundary layer wind tunnel, are used. Wind loads in tornadoes have differences compared to those in the straight-line winds. For example, Haan et al. (2010) found that the uplift coefficients on a low-rise, gable-roof building are increased by a factor of 1.8 to 3.2 in their experimental results using a tornado-vortex simulator, which was used by Amini and van de Lindt (2013) in their fragility analysis. However, this increase includes the static-pressure drop in the tornado vortex, which would not apply to net upload when there is a dominant opening in the wall or even when there is leakage (which all houses have) and the vortex core is significantly larger than the plan dimensions of the house. Thus, differences in net

Fig. 7. Cp_e variation for G6/12 and H6/12, neigh 1, suburban, 2-story house for RTWC failure.

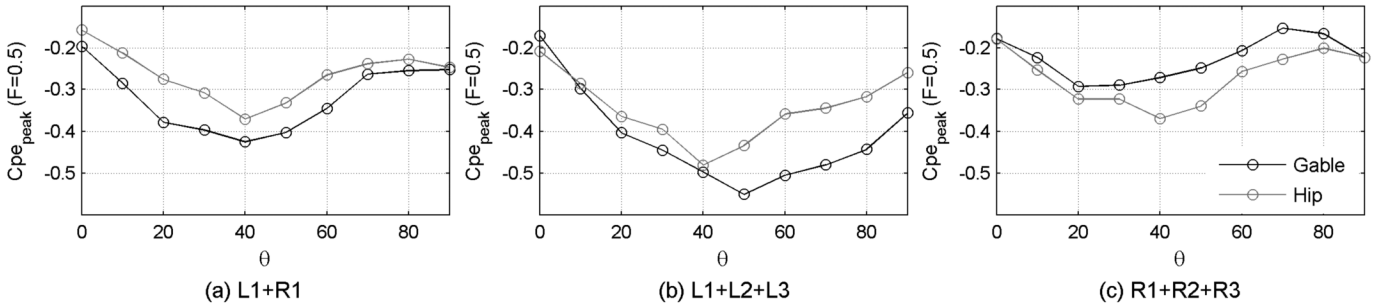

wind load coefficients applicable for roof failures are likely to be substantially smaller than the Haan et al. (2010) results suggest. In addition to differences in the spatial distribution of static-pressure, tornadoes also have significantly different vertical wind components compared to straight-line winds. Wu and Kopp (2016) found that the uplift coefficient on a flat roof building is increased by about 20% for upwardly-directed velocity fluctuations in their analysis of straight-line wind loads, which would change failure-inducing wind speeds by about 10%. However, there is no available data for gable or hip-roofed houses to assess this, including knowledge of the vertical angles of the wind in actual tornadoes. In the current work, no adjustments are made for the tornado wind field, primarily because of a lack of data, along with the above arguments. It seems probable that this assumption is reasonable for regions of tornadic wind fields outside of the vortex core where the wind direction is largely horizontal. Notwithstanding this, further work is clearly needed with respect to tornadic wind loads.

The wind load is determined as

$$W = 0.613V^2 \times (Cp_e - \gamma Cp_i) \times A_E \times \cos(\beta) \quad (3)$$

where V is the wind speed referenced to a 3 s gust wind speed measured at mean roof height, h, in the upstream terrain employed in the wind tunnel tests (i.e., open terrain, $z_0 = 0.03$ m, and suburban terrain, $z_0 = 0.23$ m), Cp_e is external pressure coefficient, and Cp_i is internal pressure coefficient. The correlation factor for peak values between Cp_e and Cp_i is γ, β is roof slope, and $0.613V^2$ is the velocity pressure calculated assuming the density of air, ρ, is 1.226 kg/m^3. The vertical component of the wind load applied for RTWC failure is obtained by multiplying by $\cos(\beta)$ in eq. (3).

The wind speed, V, defined in the EF-Scale is a 3 s gust wind speed measured at the building height, in the same terrain as the building. This is also the wind speed used in the current study. It is important to note that Kosiba and Wurman (2013) have shown using radar data that the most intense winds in a tornado could be at 5 m or lower. This is in contrast to synoptic-scale atmospheric boundary layers where the highest wind speeds are typically hundreds of metres above ground level. The effects of terrain roughness on tornadoes are unknown and likely to be different from those in the atmospheric boundary layer. Thus, it is most logical to assess the wind speeds most directly related to the failure, which for roof failures on houses would be the roof height wind speed without any adjustment for terrain, as done originally by Fujita.

The statistical information for Cp_e was calculated using the wind tunnel study of Gavanski et al. (2013). Since simultaneous wind speeds were not measured in the experiments, the measured coefficients, which were referenced to a wind tunnel mean wind speed, were converted to an equivalent 3 s gust speed reference. It is the variation of these 3 s gust-speed-referenced pressure coefficients that is used in the current paper. Implicit in this is that quasi-steady theory holds, which is reasonable for area-averages, based on the analysis of Wu and Kopp (2016). We would add that, for short duration events like this one, shorter duration gusts would likely be more representative of failure wind speeds since the wind speed is continuously and rapidly changing. This could be done using quasi-steady theory, but one would need to obtain instantaneously varying pressure coefficients by measuring pressures and wind speeds simultaneously, as done by Wu and Kopp (2016), and conduct the analysis with pressure coefficients formed with these instantaneous wind speeds. Then, a separate analysis of how the instantaneous speed relates to 3 s speeds could be conducted based on possible wind field models for the tornado. Such analyses are left to future work because of the lack of currently-available data.

Fig. 8. Cp_i variation for Angus house configuration for both RTWC and sheathing panel failure (6/12, suburban, 2-story house).

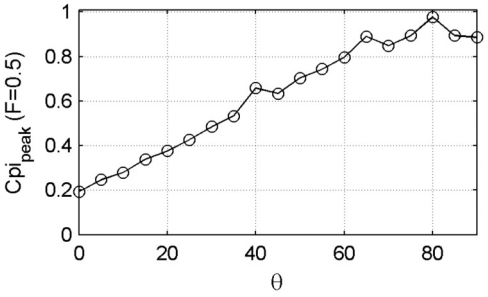

The Gavanski et al. (2013) wind tunnel study included various roof slopes (5/12, 6/12, 7/12, 9/12, 12/12), eave heights (1, 2, and 3 storeys), and terrain conditions (open, suburban) for gable- and hip-roofed houses that are both isolated and surrounded by the other houses of the same dimensions. For the global-roof-failure calculations, area-averaged pressure coefficients, Cp_{eA}, for the three combined effective tributary areas were obtained using the point pressure time histories, with peak coefficients shown in Fig. 7. For the sheathing-failure calculations, Cp_{eA} was calculated for all the possible locations of the sheathing panels on the roof considered in Gavanski et al. (2013).

The building internal pressure, Cp_i, was based on an assumed dominant opening of a size of 1.2 m × 1.2 m, typical of windows for the houses in Angus. This opening was assumed to be located near the centre of the side wall, consistent with the damage observations, which leads to the variation of Cp_i versus wind direction depicted in Fig. 8. (The area of the overhangs was included with the internal pressures, which were assumed to act on the ceiling between the living space and the attic and also on the overhangs.) The internal pressure coefficients were obtained by considering the wall-pressure time series from one of the tested models in the National Institute of Standards and Technology (NIST) aerodynamics database — see Ho et al. (2005) – with $L \times W \times h_{eave}$ = 19.1 m × 12.2 m × 5.5 m.

Both the area-averaged, external Cp_{eA}, and internal, Cp_{iA}, peak pressure coefficients are assumed to follow Gumbel distribution, which is given by:

Fig. 9. Variation of γ with respect to wind direction, θ. The solid black line is a smoothed curve fit, which is used in the current analysis.

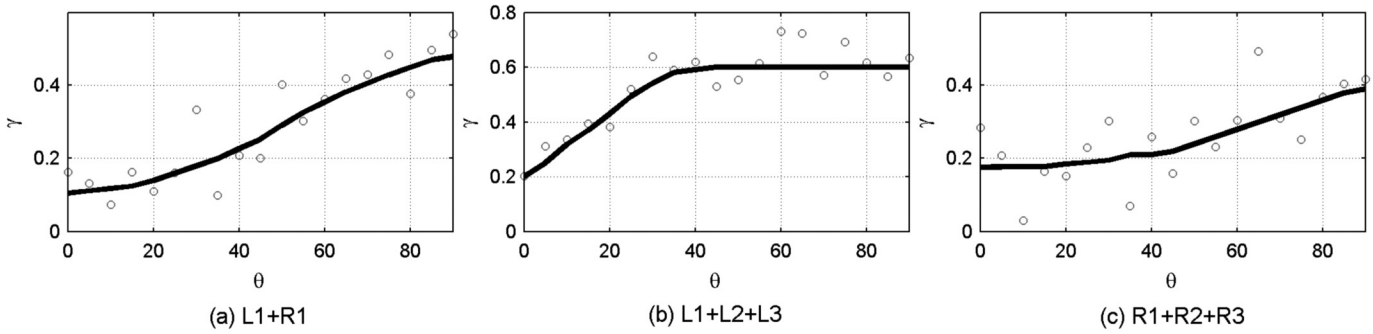

$$F(x) = \exp\{-\exp[-\alpha(x - u)]\} \quad (4)$$

where x is either Cp_{eA} or Cp_{iA}, α and u are the scale and location parameters that can be determined by the least-squares method. Figure 7 shows the peak coefficients that correspond to the 50th percentile (i.e., median) for the effective tributary areas of A_E = L1 + R1, L1 + L2 + L3, and R1 + R2 + R3.

Since the peak external and internal pressures were not measured simultaneously, the correlation between the peaks, γ, must be assessed to obtain the peak, net wind loads. To obtain γ for RTWC failure, wind tunnel data measured on the roof and walls simultaneously were utilized for this purpose, using the same data as were used to assess the internal pressure coefficients. The area-averaged Cp_e time series for the effective roof areas were cut into 10 equal segments and the minima were obtained from each segment. With Cp_{iA} time series obtained on the side wall as explained above, Cp_{iA} values corresponding to these 10 Cp_{eA} minima were selected and the mean value was calculated. This is denoted as Cp_{iAmean}. At the same time, the worst single peak was also found from Cp_{iA} time series, which is denoted as Cp_{iApeak}. Then, γ was obtained from the ratio, Cp_{iAmean}/Cp_{iApeak}. This was repeated for all wind directions and roof zones. The γ variations with wind direction for L1 + R1, L1 + L2 + L3, and R1 + R2 + R3 are presented in Fig. 9. For sheathing panel failure analysis in particular, simultaneous external and internal pressure coefficients would be useful, but are unavailable for buildings of this size, with these roof shapes. Since only the first sheathing panel failure is considered in this analysis, a constant value of $\gamma = 0.85$ regardless the location of panel and wind direction was used, based on the results from Kopp et al. (2008). This approach is consistent with existing, code-based fragility analyses of sheathing failures.

Dead load

The dead load is the weight of the components of the roof. For RTWC failure, the statistics used here are assumed to be the same as previous studies (Ellingwood et al. 2004; Li and Ellingwood 2006), i.e., the dead load is assumed to be normally distributed with a mean of 717 Pa (= D_{0mean}) and a coefficient of variation, CV, of 0.1(= D_{0CV}), using:

$$F(D) = \Phi[(D_0 - D_{0mean})/D_{0,SD}] = \Phi[(D_0 - D_{0mean})/(D_{0mean} \times D_{0CV})] \quad (5)$$

To obtain the dead load acting on A_E, the sample value of dead load, D_0, using the statistics mentioned above is multiplied with A_E. As for the sheathing panel failures, the dead load is also assumed to be normally distributed using eq. (5) but with D_{mean} = 77 Pa and D_{CV} = 0.1.

Procedure for calculating the fragility curves

A simple Monte-Carlo technique (Melchers 1999) is employed to estimate the conditional failure probability as a function of wind speed, P_f. Table 4 presents the probabilistic distributions assumed for each variable.

Table 4. Equations used to sample a normal, lognormal, Gumbel or uniform variate, X, with mean, m, and standard deviation, σ.

	Distribution	Sample of X, x
R_0	Lognormal	$x = \exp\{\ln[m/(1+v^2)^{1/2}] + [\ln(1+v^2)]^{1/2}\Phi^{-1}(p)\}$
Cp_e, Cp_i	Gumbel	$x = u + \{-\ln[-\ln(p)]\}/\alpha$
D_0	Normal	$x = m + \sigma\Phi^{-1}(p)$
θ	Uniform	x = round{[round(90*p)]/10}*10

Note: p is the standard uniformly distributed random variables between 0 and 1, and 'round' is a function to round-off to the nearest integer.

Effects of aerodynamic parameters (roof shape and neighbouring houses)

Figures 10 and 11 depict the resulting fragility curves for isolated, 2-storey houses in a suburban terrain with gable and hip roofs, respectively, with roof slopes of 6/12 and a dominant opening in the side wall. The roof slope of 6/12 was selected based on the houses observed in the damage survey in Angus. In addition, the gray range indicated in the figures is DOD-6 wind speed range. From these figures, it is clear that the roof shape has a significant effect on the failure-inducing wind speeds. For RTWC failure, the increase in the median failure wind speeds for the hip-roof compared to the gable-roof is about 50 km/h for the same effective wind area, with the gable-roof failures falling in the range of wind speeds associated with DOD-6, while the hip-roof failures tend to fall outside (above) this range, except for very low probabilities of failure. It should be emphasized that EF-Scale categories as implemented in Canada span ranges of 40 km/h, so a difference of 50 km/h is greater than one category in the EF-Scale.

To examine the effect of neighbouring houses, the fragility analysis was performed using Cp_e obtained from the isolated-house case (denoted as 'iso') as well as those obtained with surrounding houses in typical suburban patterns (denoted as 'neigh'). As noted above, four neighbouring configurations were examined; Gavanski et al. (2013) provide the precise details. Examining the results for these neighbourhood configurations, it is clear that there is little in the way of shielding effects for the roof uplift failures. This would not be the case for the horizontal drag loads. Further work on this may be required in tornado-vortex simulators, but such data are not currently available.

When the fragility curves for the RTWC and sheathing panel failures of gable roofs are compared, the curves for RTWC failure locate between the two curves for 6d-nail and 8d-nail sheathing panel failures, regardless of the neighbourhood configuration (except at high values of failure probability). Thus, if 6d nails are used for the sheathing, one would expect to see greater numbers of sheathing failures than RTWC failures (or, perhaps, RTWC failures with panels missing from the roof). However, if 8d nails are used for the sheathing, complete (gable) roof failure is more likely.

Fig. 10. Fragility curves in different neighbourhood patterns for gable-roofed 2-story houses with a roof slope of 6/12 and a dominant opening on the side wall in suburban terrain.

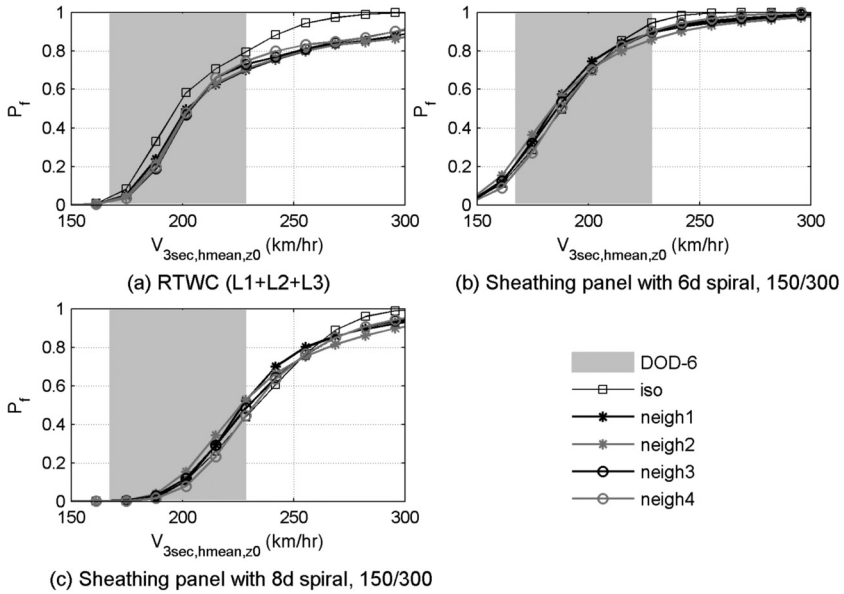

Fig. 11. Fragility curves in different neighbourhood patterns for hip-roofed 2-story houses with a roof slope of 6/12 and a dominant opening on the side wall in suburban terrain.

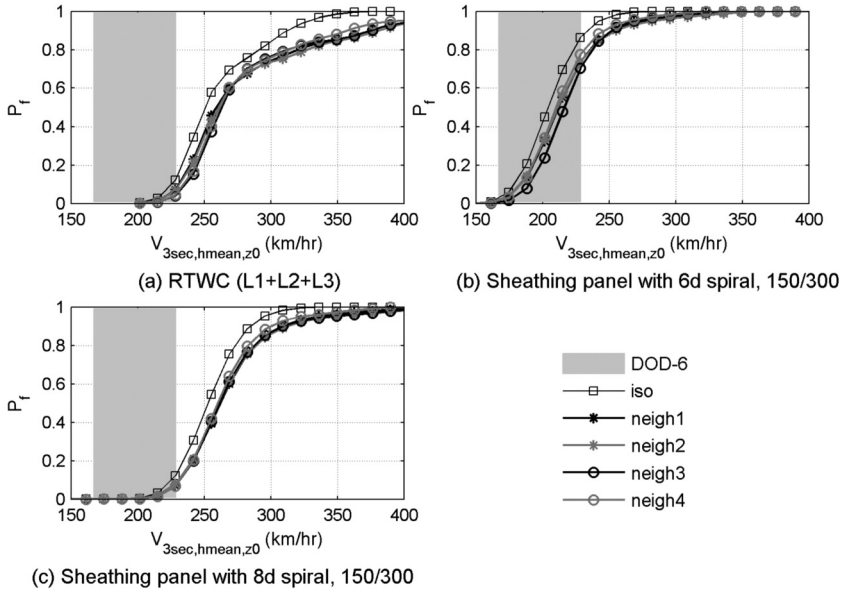

Thus, when toe-nailed connections on gable roof houses are used, the RTWCs are the weak link in the vertical load path, not the sheathing panels. Amini and van de Lindt (2013) came to a similar conclusion in their analysis. For hip-roofs, failure of 6d-nailed sheathing is most probable. However, RTWC failure probabilities are similar to those for 8d-nailed sheathing and one may expect to see similar numbers of both.

Effects of structural parameters (connection strengths and missing nails)

Based on the post-storm damage investigation of the houses in Angus, one of the possible causes for the roof failure was improperly installed RTWC fasteners. The effects of missing nails on the RTWC capacities on failure wind speed was examined by changing the R_0 information in the fragility analysis based on the tested RTWC capacity information from Morrison and Kopp (2011). RTWC using 3 toe nails will be denoted as 'perfect RTWC'. Based on Morrison and Kopp (2011) we have assumed two possible patterns for the reduction in capacity due to missing nails. One is to reduce the $R_{0\text{mean}}$ by 25% and 50% for 2-nails and 1 nail per connection, respectively (denoted as 'pattern 1'). The other is to reduce the $R_{0\text{mean}}$ by 1/3 (33%) and 2/3 (66%) for 2-nails and 1 nail per connection, respectively (denoted as 'pattern 2'). For both patterns, the standard deviation of R, $R_{0\text{SD}}$ was reduced by 20% from the perfect RTWC regardless the number of missing nails. With this information, the fragility analyses were repeated using one of the neighbourhood cases ('neigh1'), one of the combined wind effective zones (L1 + L2 + L3), and the results for gable and hip roofs with slopes of 6/12. The results are presented in Fig. 12.

The results show that missing fasteners will reduce the failure-inducing wind speeds substantially. For the gable roofs, the wind

Fig. 12. Effect of missing nails on effective wind zone of L1 + L2 + L3 of (*a*) gable- and (*b*) hip-roofed 2-story houses with a roof slope of 6/12 and a dominant opening on the side wall, surrounding by neighbouring models in suburban terrain.

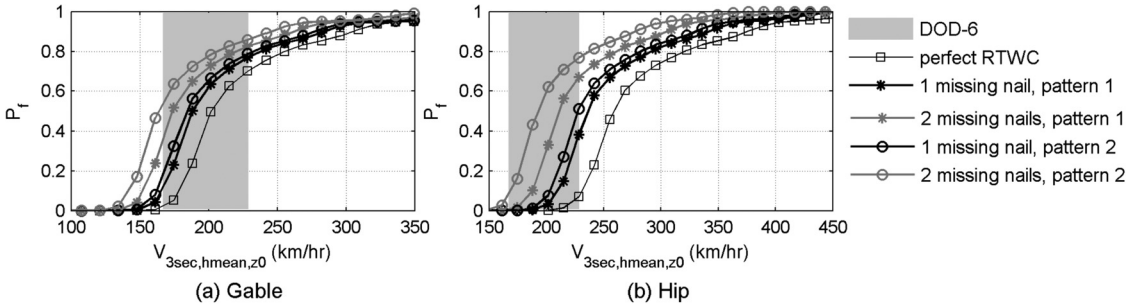

speed at the median failure probability (i.e., P_f = 0.5) is reduced from about 200 km/h for "perfect" connections to about 160–170 km/h when two nails are missing from every connection. For hip roofs, the change is more substantial, going from about 250 km/h at P_f = 0.5 to 180–200 km/h. For these types of errors, the gable roof wind speeds at P_f = 0.5 are on the lower side of the DOD-6 range (even falling below the minimum value) while those for the hip roofs (at P_f = 0.5) are in the middle of the DOD-6 range.

Wind tunnel test results for overturned trucks

Overall approach and scaling considerations

Our interest here is to assess blow-over speeds for a box truck using the failure-model approach (Surry et al. 2005; Visscher and Kopp 2007). A model of the truck was constructed with rapid prototyping methods using a length scale, $\lambda_L = L_m/L_p = 1/50$ where L is a length, the subscript, m, represents model scale, and the subscript, p, represents the prototype (i.e., full scale). The nominal size of the truck at this scale is 196 mm by 49 mm in plan and 74 mm in height. A photograph of the model is provided in Fig. 13. The mass scale ($\lambda_m = M_m/M_p$, where M is mass) can be calculated as $\lambda_M = \lambda_\rho \lambda_L^3$. Here, the density scale, $\lambda_\rho = \rho_m/\rho_p = 1$. The full-scale mass of the box truck used for the tests was assumed to be 8260 kg, which represents a fully-loaded condition. For $\lambda_L = 1/50$ and $\lambda_\rho = 1$, this leads to a model-scale mass of 66 g. It should be noted that the truck appeared to be empty before being lofted. Thus, the analysis below will consider the empty weight, which is assumed to be 5670 kg, or 45 g in model scale, i.e., 69% of the test weight.

The current work is focused on (parked) vehicle motion induced by the wind, which can be examined via the approaches used for wind-borne debris. For wind-borne debris, the most important scaling parameter for wind-induced motion of "loose-laid" objects (i.e., objects that are not fastened to a stronger underlying structure) is the ratio of the aerodynamic force to the gravitational force. Both the Tachikawa number (Holmes et al. 2006),

$$K = \frac{\rho_{air} V^2 A}{2Mg} = Fr^2 \phi \quad (6)$$

and the Froude number

$$Fr = \frac{V}{\sqrt{gL}} \quad (7)$$

measure the relative importance of these quantities. Here, ρ_{air} is the air density, V is the air (wind) velocity, A is the cross-sectional area of the object, g is the gravitational acceleration, and ϕ is a buoyancy parameter (see Baker 2007). These quantities set the scaling relationship between the velocity and length scales, as long as the density scale, $\lambda_\rho = 1$. Typically, the Froude number is used as a scaling parameter for wind loading problems where mass scaling is required (e.g., for long-span bridges) while the Tachikawa number is used for problems of wind-borne debris. Here we will use Fr for convenience. Since the gravitational acceleration cannot be scaled in wind tunnel studies, Froude number scaling implies that once the length scale is set, the velocity scale is determined by $\lambda_V = V_m/V_p = \sqrt{\lambda_L}$. Using the vehicle length scale of 1/50 yields a velocity scale of 1/7.1.

Fig. 13. Photograph of the box truck model in the wind tunnel showing the set-up for the Cobra probes and displacement transducer.

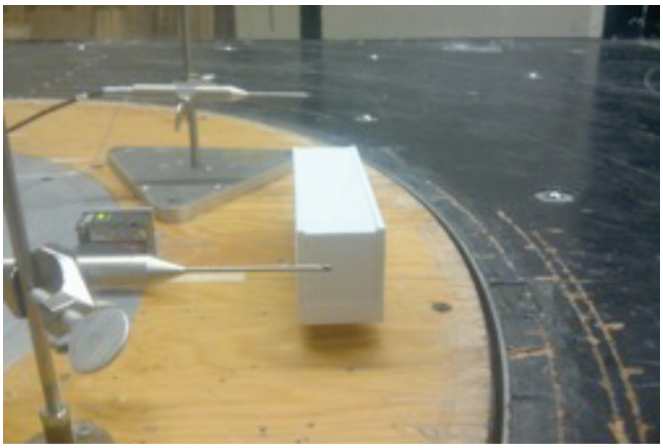

Wind tunnel simulation

The wind speed profile and turbulence intensities close to the ground in tornadoes are largely unknown, as discussed above. However, tornadoes are likely highly turbulent (although actual levels are unknown) and characterized by large swings in wind direction as they pass by. Here, two boundary layer simulations were used in Boundary Layer Wind Tunnel 1 at the University of Western Ontario to obtain overturning wind speeds for the box truck. Gust speeds at failure are measured directly, which is expected to minimize variation in the results, while the use of the two profiles provides an indication of the sensitivity to details in the flow structure and turbulence. In particular, the two wind tunnel configurations were chosen such that one had a fairly flat velocity profile while the other was rougher with higher turbulence levels. The turbulence intensities at the top of the truck (3.7 m in full scale) were 16% and 24%, respectively. The tests were conducted with the wind normal to the side of the truck, to produce the lowest failure wind speeds; however, such bluff-body shapes are not particularly sensitive to wind direction even if the wind is oblique up to ±45° (Haan et al. 2011). As well, the shifts in wind direction as a tornado passes will change so the worst case is likely to be appropriate to the analysis, given all of the other assumptions and simplifications (particularly the inability to induce lofting of the truck, which requires higher wind speeds and,

likely, a significant vertical wind component). Thus, the current results are not likely definitive, but give an indication of current understanding. They will be discussed in detail below.

Test methods and measured results

The current tests involved the overturning failure of a model truck placed on a plywood surface such that the model had the same friction coefficient as tires on asphalt. The wind tunnel speed was increased slowly until the vehicle slid or overturned, following the procedure developed by Visscher and Kopp (2007). Overturning failure was the primary mode of failure. In the simulated boundary layer flows, Cobra probe measurements were made simultaneously with a displacement transducer so that the gust speed at failure and an equivalent 3 s speed could be determined directly from the recorded data. Equivalent, 3 s gust wind speeds were obtained using the time scale relationships set by the use of the Froude scaling. Further details can be found in Stedman (2012). Twenty-five tests were conducted in each terrain configuration.

Using the Froude number scaling, the average instantaneous wind speeds at failure were 49 and 53 m/s for the two terrain conditions, with a standard deviation of about 5–6% for each. Using the time histories of wind speed measured from the Cobra probes, along with the Froude scaling, the equivalent 3 s gust speeds were found to be in the range 45–51 m/s (160–180 km/h). Assuming that the overturning moment coefficient does not change, the empty truck would have overturned at a wind speed that is 17% lower, yielding a range of 37–42 m/s (130–150 km/h). Lofting of the vehicle would be expected at higher speeds. For example, Haan et al. (2011) found in their tornado-vortex simulator study that lofting speeds for a minivan are 50% higher than overturning speeds in the same vortex.

Vehicle damage is not accounted for in the EF-Scale. In contrast, Fujita (1971) noted that vehicles can be lofted at F2, with 3 s gust wind speeds rated as 190–260 km/h (Table 2). Schmidlin et al. (2002) assessed that "semi-trucks and other high profile trucks, trailers, and buses may be tipped over" at F1 wind speeds, i.e., 125–190 km/h. Thus, the current results are consistent with those of Schmidlin et al. (2002), for the box truck both with and without a load. For lofting, the wind speeds would almost certainly be higher than the 150 km/h observed overturning of the empty truck. Since the EF-Scale in Canada has a range of 180–220 km/h for EF-2, it would appear that lofting of an empty box truck would occur in the upper EF-1 and perhaps into the EF-2 range of wind speeds given Haan et al.'s (2011) findings. Further work on lofting vehicles using tornado-vortex simulators will be needed to resolve the uncertainty with respect to this issue, particularly because of the vertical component of the wind, which may have been augmented at the location of the truck by the presence of the house. In the next section we address the correlation between this failure and those observed on the adjacent houses.

Discussion

Global roof failures – DOD-6

Fujita noted that "roofs are torn off frame houses" at F2 with a range of wind speeds of 190–260 km/h. Roof failures of wood-frame houses correspond to DOD-6, which has been given a range of 165–230 km/h in the EF-Scale with an 'expected' value of 195 km/h. Comparing the Fujita and Enhanced-Fujita Scales, the F2 range spans EF-2 and EF-3, with EF-2 in Canada being 180–220 km/h and EF-3 being 225–265 km/h. Considering the range of failure wind speeds found in the current fragility analyses, along with the discussion in the original EF-Scale documentation (WSEC 2006, which states that the range for DOD-6 spans from a low end with errors in construction to performance of roofs with hurricane straps at the high end), it would appear that the EF-Scale DOD wind speeds should be interpreted as average or median values. Otherwise, the ranges of failure wind speeds associated for each DOD for each Damage Indicator make little sense.

Considering the current fragility analysis, the median value for gable roofs with code-based, toe-nailed RTWCs is about 200 km/h (Fig. 10). For hip roofs it is about 260 km/h (Fig. 11). Thus, the current analysis indicates that the EF-Scale is appropriate for gable roofs, but underestimates the failure-inducing wind speeds for global failure of hip roofs even with Environment Canada's (2013) added note to use the upper end of the range (i.e., 230 km/h) for hip roofs. Interestingly, Fujita's original scale appears to give closer values. While wind tunnel tests in tornado-like vortex flows would be desirable to confirm such results, particularly to account for the vertical component of the wind, it appears likely that the EF-Scale DIs should distinguish between these roof shapes for wood-frame houses.

As discussed in the introduction, the EF-Scale (WSEC 2006) report discusses the effects of missing fasteners, such that the effects of missing fasteners imply that the lower bound for DOD-6 should be used, i.e., 165 km/h. The current results suggest that the lower bound of 165 km/h for DOD-6 is reasonable for a typical or average failure wind speed, with median values of about 160–170 km/h found for the case of two missing nails on gable roofs (Fig. 12), while being higher for hip roofs (180–200 km/h; Fig. 12). Thus, the lower bound speed for DOD-6 appears to be sufficiently accurate to deal with errors for gable roofs, while the expected value for the current DOD-6 applies to hip roofs with significant errors in the toe-nailed connections.

Correlation between DOD-4 and box-truck lofting

As noted above, overturning of an empty box truck likely occurs in the range of speeds from about 130 to 150 km/h. Higher speeds are expected for lofting of a box truck, which was observed in the Angus event. Adjacent to the truck failure are several houses with DOD-4 damage including roof sheathing failures and the inward collapse of garage doors. Figures 10 and 11 indicate that the wind speed for the median probability of failure for sheathing fastened with 8d nails is about 230 km/h for gable roofs and 260 km/h for hip roofs, assuming that there are no missing nails. These speeds appear to be considerably higher than the range of wind speeds for the box truck failure, and suggesting that the 'expected' value of 155 km/h for DOD-4 may be low for sheathing for panels with no errors, noting that no assessment could be made of missing nails in the damage survey. Further research on this seems warranted, in particular the effect of the vertical components of the wind on sheathing performance.

Conclusions

The damage observed in the Angus tornado is consistent with the EF-2 category, based on complete roof failures of wood-frame houses. The post-storm field survey indicated that much of the structural roof and wall damage was associated with poor construction quality caused by missing toe-nails in the roof-to-wall connections and nails in the inter-story wall-to-floor connections. However, a fragility analysis of these failures, which considered the effects of missing nails, suggests that this tornado had wind speeds in the EF-2 range. The results of the fragility analysis also suggest that the wind speeds associated with various DIs/DODs should be associated with median failure probabilities since the wide range of wind speeds associated with the full range of wind speeds exceed the ranges provided in the EF-Scale. In addition, the Environment Canada modification of DOD-6 wind speeds for failure of wood-frame roofs, which indicates higher values for hip roofs, is well justified, although the current analysis indicates higher wind speeds still. A lofted and overturned U-Haul box truck was also observed in the field survey to be well correlated with repetitive shingle, roof sheathing, and garage door failures. These conclusions are based on an analysis of boundary layer wind tunnel results, which likely only apply away from the core of vortex in the region where the wind directions are primarily horizontal.

Further research is needed using tornado-vortex simulators to determine the effects of the vertical component of the wind on roof failures, in particular.

Acknowledgements

This work was financially supported by NSERC and the Institute for Catastrophic Loss Reduction (ICLR). The ongoing interest and support of Mr. Paul Kovacs is gratefully acknowledged. The authors also acknowledge the support provided by Ms. Sarah Stenabaugh and Mr. Chieh-Hsun Wu in conducting the damage survey.

References

Amini, M., and van de Lindt, J. 2013. Quantitative insight into rational tornado design wind speeds for residential wood frame structures using a fragility approach. Journal of Structural Engineering, **140**(7): 04014033. doi:10.1061/(ASCE)ST.1943-541X.0000914.

Baker, C.J. 2007. The debris flight equations. Journal of Wind Engineering and Industrial Aerodynamics, **95**: 329–353. doi:10.1016/j.jweia.2006.08.001.

Bunting, W.F., and Smith, B.E. 1993. A guide for conducting convective windstorm surveys. NOAA Technical Memorandum NWS SR-146, United States Department of Commerce, 42 pages.

Cheng, J. 2004. Testing and analysis of the toe-nailed connection in the residential roof-to-wall-system. Forrest Products Journal, **54**(4): 58–65.

Ellingwood, B.R., Rosowsky, D.V., Li, Y., and Kim, J.H. 2004. Fragility assessment of light-frame wood construction subjected to wind and earthquake hazards. Journal of Structural Engineering, **130**(12): 1921–1930. doi:10.1061/(ASCE)0733-9445(2004)130:12(1921).

Environment Canada. 2013. Enhanced Fujita Scale (EF-Scale). Available from http://ec.gc.ca/meteo-weather/default.asp?lang=En&n=41E875DA-1 [accessed 11 November 2013].

Fujita, T.T. 1971. Proposed characterization of tornados and hurricanes by area and intensity. Satellite and Mesometeorology Research project Report 91, University of Chicago, Chicago, IL, USA.

Gavanski, E., Kordi, B., Kopp, G.A., and Vickery, P.J. 2013. Wind loads on roof sheathing of houses. Journal of Wind Engineering and Industrial Aerodynamics, **114**: 106–121. doi:10.1016/j.jweia.2012.12.011.

Gavanski, E., Kopp, G.A., and Hong, H.P. 2014. Reliability analysis of roof sheathing panels on wood-frame houses under wind loads in Canadian cities. Canadian Journal of Civil Engineering, **41**: 717–727. doi:10.1139/cjce-2013-0549.

Haan, F.L., Balaramudu, V.K., and Sarkar, P.P. 2010. Tornado-induced wind loads on a low-rise building. Journal of Structural Engineering, **136**(1): 106–116. doi:10.1061/(ASCE)ST.1943-541X.0000093.

Haan, F.L., Sarkar, P.P., and Kopp, G.A. 2011. Using physical simulations to quantify critical velocities for tornado-induced vehicle movement. Proceedings of the 13th International Conference on Wind Engineering, Amsterdam.

Henderson, D.J., Morrison, M.J., and Kopp, G.A. 2013. Response of toe-nailed, roof-to-wall connections to extreme wind loads in a full-scale, timber-framed, hip roof. Engineering Structures, **56**: 1474–1483. doi:10.1016/j.engstruct.2013.07.001.

Ho, T.C.E., Surry, D., Morrish, D., and Kopp, G.A. 2005. The UWO contribution to the NIST aerodynamic database for wind loads on low buildings: Part 1. Archiving format and basic aerodynamic data. Journal of Wind Engineering and Industrial Aerodynamics, **93**(1): 1–30. doi:10.1016/j.jweia.2004.07.006.

Holmes, J.D., Baker, C.J., and Tamura, Y. 2006. Tachikawa number: A proposal. Journal of Wind Engineering and Industrial Aerodynamics, **94**(1): 41–47. doi:10.1016/j.jweia.2005.10.004.

Insurance Bureau of Canada. 2014. Available at http://www.ibc.ca/on/resources/media-centre/media-releases/angus-ontario-tornado-costs-over-$30-million-in-insured-damage. [date accessed: 2016 April 22.]

Jensen, M. 1958. The model law for phenomena in the natural wind. Ingenioren, Int. Ed. 2.

Khan, M.A.A., Morrison, M.J., Henderson, D.J., and Kopp, G.A. 2012. Damage accumulation and load sharing in residential, wood-frame, roofs under fluctuating wind loads. *In* Proceedings of EMI Annual Conference, Notre Dame, Indiana, USA.

Kopp, G.A., Oh, J.H., and Inculet, D.R. 2008. Wind-induced internal pressures in houses. Journal of Structural Engineering, **134**: 1129–1138. doi:10.1061/(ASCE)0733-9445(2008)134:7(1129).

Kopp, G.A., Morrison, M.J., and Henderson, D.J. 2012. Full-scale testing of low-rise, residential buildings with realistic wind loads. Journal of Wind Engineering and Industrial Aerodynamics, **104–106**: 25–39. doi:10.1016/j.jweia.2012.01.004.

Kosiba, K.A., and Wurman, J. 2013. The three-dimensional structure and evolution of a tornado boundary layer. Weather and Forecasting, **28**: 1552–1561. doi:10.1175/WAF-D-13-00070.1.

Li, Y., and Ellingwood, B.R. 2006. Hurricane damage to residential construction in the US: Importance of uncertainty modeling in risk assessment. Engineering Structures, **28**: 1009–1018. doi:10.1016/j.engstruct.2005.11.005.

Mehta, K. 2013. Development of the EF-Scale for Tornado Intensity. Journal of Disaster Research, **8**(6): 1034–1041. doi:10.20965/jdr.2013.p1034.

Melchers, R.E. 1999. Structural reliability analysis and prediction (2nd edition). Chichester, West Sussex, England: John Wiley and Sons Ltd.

Morrison, M.J., and Kopp, G.A. 2011. Performance of toe-nail connections under realistic wind loading. Engineering Structures, **33**: 69–76. doi:10.1016/j.engstruct.2010.09.019.

Morrison, M.J., Henderson, D.J., and Kopp, G.A. 2012. The response of a wood-frame, gable roof to fluctuating wind loads. Engineering Structures, **41**: 498–450. doi:10.1016/j.engstruct.2012.04.002.

Morrison, M.J., Kopp, G.A., Gavanski, E., Miller, C., and Ashton, A. 2014. Assessment of damage to residential construction from the tornadoes in Vaughan, Ontario, on 20 August 2009. Canadian Journal of Civil Engineering, **41**(6): 550–558. doi:10.1139/cjce-2013-0570.

NBCC. 2010. National Building Code of Canada, Canadian Commission on Building and Fire Codes, National Research Council Canada, Ottawa, Ont.

Rosowsky, D.V., and Cheng, N. 1999. Reliability of light-frame roofs in high-wind regions. I: wind loads. Journal of Structural Engineering, **125**(7): 725–733. doi:10.1061/(ASCE)0733-9445(1999)125:7(725).

Roueche, D.B., and Prevatt, D.O. 2013. Residential damage patterns following the 2011 Tuscaloosa, AL and Joplin, MO Tornadoes. Journal of Disaster Research, **8**: 1061–1067. doi:10.20965/jdr.2013.p1061.

Schmidlin, T., Hammer, B., King, P., Ono, Y., Miller, L.S., and Thumann, G. 2002. Unsafe at Any (Wind) Speed? Bulletin of the American Meteorological Society, **83**. doi:10.1175/BAMS-83-12-1821.

Schwarz, G.E. 1978. Estimating the dimension of a model. The Annals of Statistics, **6**(2): 461–464. doi:10.1214/aos/1176344136.

Shanmugam, B., Nielson, B.G., and Prevatt, D.O. 2009. Statistical and analytical models for roof components in existing light-framed wood structures. Engineering Structures, **31**: 2607–2616. doi:10.1016/j.engstruct.2009.06.009.

Sills, D.M.L., McCarthy, P.J., and Kopp, G.A. 2014. Implementation and application of the EF-scale in Canada. *In* Extended Abstracts, 27th AMS Conference on Severe Local Storms, Madison, WI, American Meteorological Society, Paper 16B.6.

Stedman, D. 2012. Wind-tunnel tests of model vehicles to determine failure-inducing tornado wind speeds. 4th year thesis, Department of Civil and Environmental Engineering, University of Western Ontario, London, ON, Canada.

Storm Prediction Center (SPC). 2016. The Enhanced Fujita Scale (EF Scale). Available from http://www.spc.noaa.gov/efscale/ [accessed 21 September 2016].

Surry, D. 1999. Wind loads on low-rise buildings: past, present and future. *In* 10th International Conference on Wind Engineering, Copenhagen, Denmark, pp. 105–114.

Surry, D., Kopp, G.A., and Bartlett, F.M. 2005. Wind load testing of low buildings to failure at model and full scale. Natural Hazards Review, **6**: 121–128. doi:10.1061/(ASCE)1527-6988(2005)6:3(121).

Visscher, B., and Kopp, G.A. 2007. Trajectories of roof sheathing panels under high winds. Journal of Wind Engineering and Industrial Aerodynamics, **95**: 697–713. doi:10.1016/j.jweia.2007.01.003.

Wind Science and Engineering Center (WSEC). 2006. A recommendation for an Enhanced Fujita Scale. Texas Tech University, Lubbock, TX, USA.

Wu, C.-H., and Kopp, G.A. 2016. Estimation of wind-induced pressures on a low-rise building using quasi-steady theory. Frontiers in Built Environments, **14**. doi:10.3389/fbuil.2016.00005.